12-2002

An Observational Test of the Spherical Model Atmospheres for the M Class Giants: The Case of δ2 Lyrae

Jeffrey J. Sudol
West Chester University of Pennsylvania, jsudol@wcupa.edu

J. A. Benson
U.S. Naval Observatory, Flagstaff Station, AZ

H. M. Dyck
U.S. Naval Observatory, Flagstaff Station, AZ

M. Scholz
Universitat Heidelberg

The Astronomical Journal, 124:3370–3378, 2002 December

AN OBSERVATIONAL TEST OF THE SPHERICAL MODEL ATMOSPHERES FOR THE M CLASS GIANTS: THE CASE OF δ^2 LYRAE

J. J. Sudol
National Solar Observatory, GONG Project, P.O. Box 26732, Tucson, AZ 85726-6732; jsudol@noao.edu

J. A. Benson and H. M. Dyck
US Naval Observatory, Flagstaff Station, P.O. Box 1149, Flagstaff, AZ 86002-1149;
meldyck@sextans.lowell.edu, jbenson@sextans.lowell.edu

and

M. Scholz
Institut für Theoretische Astrophysik, Universität Heidelberg, Tiergartenstrasse 15, D-69121 Heidelberg, Germany;
and School of Physics, University of Sydney, Sydney, NSW 2006, Australia; scholz@ita.uni-heidelberg.de
Received 2002 February 19; accepted 2002 August 28

ABSTRACT

We have obtained interferometric data for δ^2 Lyrae, spectral type M4 II, at 1.25 and 1.65 μm at the Navy Prototype Optical Interferometer. This star has also been observed at the Mark III Optical Interferometer at optical wavelengths and at the Infrared-Optical Telescope Array at 2.20 μm. These observations have resulted in a total of seven uniform-disk diameter (UDD) estimates for δ^2 Lyrae at seven wavelengths. We compare the UDD estimates for δ^2 Lyrae to the most recent, static, M class giant model atmospheres. The most appropriate model that we can construct for δ^2 Lyrae, matching the star in mass, radius, and luminosity, cannot account for the observed variations in the UDDs with wavelength. Among 18 alternate models, the model that provides the best fit to the data has almost the same $T_{\rm eff}$ as δ^2 Lyrae but a lower mass and a more extended atmosphere. None of the models investigated, however, appear to provide a satisfactory description of the atmosphere of δ^2 Lyrae. We discuss several possible explanations for these results and the implications of the relative success of the lower mass model.

Key words: stars: late-type — stars: AGB and post-AGB — stars: atmospheres — stars: individual (δ^2 Lyrae) — instrumentation: interferometers — techniques: interferometric

1. INTRODUCTION

The development of sensitive optical and infrared Michelson interferometers has made possible new observational tests of model atmospheres of the M class giants. These stars have been among the last to yield to model predictions owing to the large quantity of laboratory data needed to account for the opacities of all of the atomic and molecular species present in the atmospheres of these stars and owing to modeling problems resulting from the substantial geometric extension of the atmosphere. The application of model atmospheres to hotter stars appears to be under much better control. For example, Quirrenbach et al. (1996) have demonstrated that the observed variations in the uniform-disk diameters (UDDs) for α Bootis ($T_{\rm eff} = 4500$ K) with wavelength between 0.45 and 2.20 μm are in agreement with the predictions of plane-parallel model atmospheres. Hanbury Brown et al. (1974b) have demonstrated agreement between the visibility data for α Canis Majoris ($T_{\rm eff} = 10{,}000$ K), obtained at the Narrabri Intensity Interferometer, and a plane-parallel model atmosphere for that star, and Hajian et al. (1998) have demonstrated agreement between triple-amplitude data for α Arietis ($T_{\rm eff} = 4450$ K), and α Cassiopeiae ($T_{\rm eff} = 4800$ K), obtained at the Navy Prototype Optical Interferometer (NPOI), and Kurucz model atmospheres for those stars (Kurucz 1979).

In the course of the past 15 years, several series of low-temperature (2500 K $< T_{\rm eff} <$ 3800 K), spherically extended model atmospheres have been developed for the static M class giants (Scholz 1985; Scholz & Takeda 1987; Bessell et al. 1989a, 1991; Hofmann & Scholz 1998) and the M class Mira variables (Scholz & Takeda 1987; Bessell et al. 1989b; Bessell, Scholz, & Wood 1996; Hofmann, Scholz, & Wood 1998). The models include opacity contributions from molecular species known to be important from the spectra of cool stars. Bessell et al. (1989a) found satisfactory agreement between the colors and effective temperatures of the static M class giant models and the observed colors and temperatures of the M class giants, bolstering confidence in the models as good representations of real M class giant atmospheres. Bessell et al. (1989b) found satisfactory agreement between a number of the observable properties of the M class Mira models and the Mira variables as well. Completely satisfactory agreement between the models and the interferometric data for the Mira variables, however, has not been achieved (e.g., Haniff, Scholz, & Tuthill 1995; Weigelt et al. 1996; Perrin et al. 1999; Hofmann et al. 2000, 2001), and the models have not yet been compared to interferometric data for small amplitude ($\Delta m \lesssim 1.0$), red variable stars, such as δ^2 Lyrae, or nonvariable M class giants.

Three products of the model computations are of interest to us in this paper: the center-to-limb variation (CLV) in the intensity of the radiation emitted in the direction of the observer in each passband defined in the model, the "filter radius" in each passband, and the Rosseland radius. Interferometric data are sensitive to the shape of the CLV, which depends on the temperature-density stratification of the atmosphere and the opacity of the material in the atmosphere (e.g., Baschek, Scholz, & Wehrse 1991). The filter radius, $R_{\rm fil}$, associated with a particular passband is a

weighted mean of the monochromatic radii in that passband (e.g., Scholz & Takeda 1987). The monochromatic radius, R_λ, at a given wavelength, λ, is defined to be the distance from the center of the star to the layer at which $\tau_\lambda = 1$. The Rosseland radius is the distance from the center of the star to the layer at which the Rosseland mean optical depth reaches unity ($\tau_{\rm Ross} = 1$). The Rosseland radius is a common choice for "the radius" of a star in stellar atmosphere research because the Rosseland mean optical depth is independent of wavelength and because the Rosseland mean optical depth scale is used to tie the deep atmospheric layers to the interior model.

Although the Michelson interferometer is a promising instrument for obtaining the data from which a stellar CLV can be reconstructed, interferometers have not matured to the point that this can be done. Current limitations include the precision of the visibilities and the extent of the sampling in the Fourier domain, which depends on the number of apertures in the interferometer. It is customary, therefore, to fit a uniform disk to the interferometric data for a particular star to arrive at an estimate of the angular diameter of the stellar disk (e.g., Davis, Tango, & Booth 2000). Although the uniform-disk fit depends on just one parameter, the angular diameter of the disk, the result is sensitive to the fitting technique, a subject to which we return in § 2. Stellar disks are not uniform disks, of course, so it is customary to scale the result of the fit, the UDD, to some well-defined diameter, such as the Rosseland mean diameter (RMD). The scaling and the resulting diameter depend on the choice of the model.

To allow for observational tests of the model atmospheres for the M class giants, Hofmann & Scholz (1998) fit uniform disks to the CLVs in each of 12 photometric passbands for 18 model atmospheres. The results of these fits are the ratios of the uniform-disk radii to the filter radii ($R_{\rm UD}/R_{\rm fil}$) listed in Table 2 in their paper. The ratios of the filter radii to the Rosseland radii ($R_{\rm fil}/R_{\rm Ross}$) are products of the model computations; these ratios are also listed in Table 2 in their paper. The product of these two ratios in a particular passband provides the scaling between the Rosseland radius and a uniform-disk radius, which ties the observations to the model.

A number of objections to using the uniform-disk model can be raised. Hofmann & Scholz (1998) have noted that the fully darkened disk (FDD) model often provides better fits to the M class giant model CLVs than the uniform-disk model, and Davis et al. (2000) have recommended direct comparisons of the Fourier transforms of the model CLVs and the interferometric data in those cases where the data are quite precise (better than 1%) and the limb darkening is severe. For this project, however, we are using the results of interferometric observations available in the literature. In the relevant citations, FDDs are not fitted to the data and the original data are not presented. UDD results are universal, so we have chosen to work with UDDs in this paper. We discuss some of the limitations of our data set in § 4.

The work of Hofmann & Scholz (1998) lends itself to the following observational test of the models. UDDs in several passbands are obtained for a particular star from interferometric observations. These UDDs are then scaled to RMDs as prescribed by the most appropriate model for the star. (Following the scheme developed by Hofmann & Scholz, the product of the ratio of the uniform-disk radius to the filter radius, $R_{\rm UD}/R_{\rm fil}$, and the ratio of the filter radius to the Rosseland radius, $R_{\rm fil}/R_{\rm Ross}$, is the ratio of the uniform-disk radius to the Rosseland radius, $R_{\rm UD}/R_{\rm Ross}$. Dividing this result into the UDD gives the RMD.) Because the RMD is a wavelength-independent quantity, the RMDs at all wavelengths ought to agree with one another to within their uncertainties if the model is a good representation of the atmosphere of the star. The wavelength independence of the RMD provides a robust test of the quality of the limb-darkening in the model. Bandpasses with large $R_{\rm fil}/R_{\rm Ross}$ ratios, those in which strong absorption features dominate, are expected to be more sensitive to the structure of the model than bandpasses with small $R_{\rm fil}/R_{\rm Ross}$ ratios.

We have gathered together in this paper the UDDs for δ^2 Lyrae resulting from all published interferometric observations to date, and we have added to this data set UDDs resulting from observations at 1.25 and 1.65 μm obtained at the NPOI. In total, we have available to us UDDs at seven wavelengths across the optical and the near-infrared, more UDDs at more wavelengths than are available for any other source.

The star δ^2 Lyrae is a small amplitude ($\Delta m_v \approx 0.20$), red variable (Bakos & Tremko 1991). The spectral classification in the MK system is M4 II (Morgan & Keenan 1973). The effective temperature is near 3500 K (e.g., Dyck, van Belle, & Thompson 1998), and prior observations indicate the atmosphere is extended (Quirrenbach et al. 1993). We discuss the properties of δ^2 Lyrae in greater detail in § 3, but for now we want to note that it represents the best observed M class giant to date against which to test the non-Mira M class giant model atmospheres.

2. OBSERVATIONS

We have obtained interferometric data for δ^2 Lyrae at 1.25 μm ($\Delta\lambda = 0.30$ μm, where $\Delta\lambda$ represents the FWHM filter bandwidth) and 1.65 μm ($\Delta\lambda = 0.30$ μm) using the Navy Prototype Optical Interferometer (NPOI). A journal of the observations appears in Table 1. For a description of the interferometer, we refer the reader to Armstrong et al. (1998). The NPOI is designed to operate at optical wavelengths between 0.45 and 0.85 μm. In order to conduct observations at near-infrared wavelengths, we added to the interferometer near-infrared beam-combining optics and a single-element InSb detector. The detector is one of the two detectors previously used at the Infrared-Optical Telescope Array (IOTA; Dyck et al. 1995) and at the Infrared Michelson Array (IRMA; Dyck, Benson, & Ridgway 1993). Having just one detector, we limited observations to a single baseline between the center and west astrometric siderostats. These two siderostats form a 22.199 m baseline at a position angle of 63°.64 east of north. Descriptions of the near-infrared instrument, data reduction, data calibration, and the UDD fits to the data for δ^2 Lyrae follow.

2.1. *The Near-infrared Instrument*

Within the beam-combining laboratory at the NPOI, the beams from each siderostat are split into separate optical and near-infrared beams at a dichroic. The optical beams are fed to the NPOI narrow-angle trackers. The near-infrared beams are combined, and the combined beam is focused onto the InSb detector.

With the equipment available, we could not fringe track at near-infrared wavelengths. We developed new software

TABLE 1

JOURNAL OF THE OBSERVATIONS OF α LYRAE AND δ^2 LYRAE AND RESULTING VISIBILITY DATA

Source	λ (μm)	s	V_i	V_α	V_δ
			1998 Jul 1		
α Lyrae	1.25	74.55	0.1706 ± 0.0068	0.1828 ± 0.0111	
δ^2 Lyrae.....	1.25	75.98	0.0840 ± 0.0027		0.460 ± 0.035
α Lyrae	1.25	80.18	0.1685 ± 0.0079	0.1825 ± 0.0120	
δ^2 Lyrae.....	1.25	79.50	0.0765 ± 0.0026		0.419 ± 0.033
α Lyrae	1.25	82.31	0.1996 ± 0.0087	0.2171 ± 0.0137	
δ^2 Lyrae.....	1.25	81.93	0.0790 ± 0.0025		0.364 ± 0.028
α Lyrae	1.25	85.24	0.2208 ± 0.0076	0.2417 ± 0.0138	
δ^2 Lyrae.....	1.25	84.08	0.0747 ± 0.0027		0.309 ± 0.023
α Lyrae	1.25	85.79	0.2226 ± 0.0072	0.2440 ± 0.0136	
δ^2 Lyrae.....	1.25	85.03	0.0696 ± 0.0025		0.285 ± 0.021
α Lyrae	1.25	86.09	0.2400 ± 0.0057	0.2632 ± 0.0136	
δ^2 Lyrae.....	1.25	86.06	0.0693 ± 0.0024		0.263 ± 0.018
			1998 Jul 2		
α Lyrae	1.25	84.25	0.1795 ± 0.0059	0.1961 ± 0.0110	
δ^2 Lyrae.....	1.25	83.93	0.0585 ± 0.0025		0.298 ± 0.023
α Lyrae	1.25	85.59	0.1525 ± 0.0077	0.1671 ± 0.0114	
δ^2 Lyrae.....	1.25	85.48	0.0529 ± 0.0020		0.317 ± 0.026
α Lyrae	1.25	86.09	0.1532 ± 0.0063	0.1680 ± 0.0103	
δ^2 Lyrae.....	1.25	86.08	0.0535 ± 0.0021		0.318 ± 0.025
α Lyrae	1.25	85.98	0.1677 ± 0.0055	0.1839 ± 0.0104	
δ^2 Lyrae.....	1.25	86.00	0.0568 ± 0.0019		0.309 ± 0.022
			1998 Jul 11		
α Lyrae	1.65	62.83	0.3563 ± 0.0085	0.3743 ± 0.0193	
δ^2 Lyrae.....	1.65	62.54	0.1949 ± 0.0053		0.521 ± 0.034
α Lyrae	1.65	63.82	0.3412 ± 0.0071	0.3590 ± 0.0181	
δ^2 Lyrae.....	1.65	63.53	0.2025 ± 0.0041		0.564 ± 0.035
α Lyrae	1.65	64.62	0.3438 ± 0.0085	0.3622 ± 0.0188	
δ^2 Lyrae.....	1.65	64.33	0.1942 ± 0.0040		0.536 ± 0.034
α Lyrae	1.65	64.86	0.3227 ± 0.0071	0.3401 ± 0.0173	
δ^2 Lyrae.....	1.65	64.66	0.1896 ± 0.0044		0.557 ± 0.035
α Lyrae	1.65	65.17	0.3409 ± 0.0080	0.3595 ± 0.0185	
δ^2 Lyrae.....	1.65	65.21	0.1907 ± 0.0050		0.531 ± 0.035
α Lyrae	1.65	65.06	0.3324 ± 0.0083	0.3504 ± 0.0183	
δ^2 Lyrae.....	1.65	65.14	0.1763 ± 0.0049		0.503 ± 0.033
α Lyrae	1.65	63.98	0.2948 ± 0.0075	0.3103 ± 0.0162	
δ^2 Lyrae.....	1.65	64.12	0.1822 ± 0.0043		0.587 ± 0.038
α Lyrae	1.65	63.11	0.2830 ± 0.0064	0.2974 ± 0.0152	
δ^2 Lyrae.....	1.65	63.25	0.1653 ± 0.0039		0.556 ± 0.035
α Lyrae	1.65	61.53	0.3263 ± 0.0072	0.3421 ± 0.0174	
δ^2 Lyrae.....	1.65	61.57	0.1800 ± 0.0062		0.526 ± 0.036
α Lyrae	1.65	60.03	0.2967 ± 0.0099	0.3103 ± 0.0176	
δ^2 Lyrae.....	1.65	59.77	0.1928 ± 0.0064		0.621 ± 0.045
α Lyrae	1.65	59.13	0.3062 ± 0.0076	0.3198 ± 0.0167	
δ^2 Lyrae.....	1.65	58.92	0.2156 ± 0.0064		0.674 ± 0.045
			1998 Jul 12		
α Lyrae	1.65	65.10	0.3586 ± 0.0061	0.3781 ± 0.0185	
δ^2 Lyrae.....	1.65	65.18	0.2128 ± 0.0034		0.563 ± 0.034
α Lyrae	1.65	64.27	0.3713 ± 0.0060	0.3909 ± 0.0190	
δ^2 Lyrae.....	1.65	64.44	0.2150 ± 0.0041		0.550 ± 0.033
α Lyrae	1.65	63.22	0.3822 ± 0.0069	0.4017 ± 0.0198	
δ^2 Lyrae.....	1.65	63.39	0.2260 ± 0.0047		0.563 ± 0.035
α Lyrae	1.65	61.72	0.3994 ± 0.0069	0.4188 ± 0.0205	
δ^2 Lyrae.....	1.65	61.82	0.2380 ± 0.0045		0.568 ± 0.034
α Lyrae	1.65	60.37	0.3887 ± 0.0086	0.4068 ± 0.0207	
δ^2 Lyrae.....	1.65	60.34	0.2460 ± 0.0049		0.605 ± 0.038

NOTES.—The spatial frequency, s, is given in cycles per arcsecond. V_i represents the instrumental visibility of the source. V_α represents the visibility of α Lyrae corrected for partial resolution. V_δ represents the calibrated visibility for δ^2 Lyrae.

to control two of the six NPOI "fast delay line" carts to create "fringe packets." The software holds one cart fixed in position while driving the other cart back and forth through the position of the white light fringe. A single observation consists of 47 "ramps" in the cart motion; each ramp is 4 s in duration. During each ramp, the cart is driven at such a rate as to produce 100 Hz interference fringes. A single fringe packet is constructed in 80 ms at 1.25 μm and 110 ms at 1.65 μm. The recorded interference fringes are similar to those recorded at IOTA (Dyck et al. 1995).

The detector signal is passed through a combination of two amplification stages and three filter stages then digitized through a 12-bit analog-to-digital converter on board a local PC. The amplification and filter electronics are designed to minimize the signal noise without compromising the fidelity of the fringe packet and to scale the signal to lie within the appropriate voltage range for the analog-to-digital converter.

2.2. *Data Reduction*

We developed new software to reduce the data obtained with the near-infrared instrument. Our data reduction procedure is an adaptation of the procedure developed for the IRMA project (Benson, Dyck, & Howell 1995). One-second sections of the recorded signal, each containing a fringe packet, are stripped from the signal. The power spectrum for each fringe packet is computed, then filtered. Filtering occurs in two stages. First, all of the power at those frequencies outside a 48 Hz bandwidth centered on 100 Hz (the frequency of the interference fringes) is removed (set to zero), then an estimate of the noise power at those frequencies inside the bandwidth is subtracted from the power spectrum. The noise power estimate is constructed from 1 s sections of the recorded signal adjacent to, but not including, the fringe packets. The filtered power spectrum for each fringe packet is reduced to an amplitude spectrum. In the process, the sign of the power is preserved. The inverse transform of the amplitude spectrum is then computed. The first point in the inverse transform of the amplitude spectrum is taken to be the visibility of the fringe packet.

Each observation results in a signal containing 47 fringe packets. The visibilities of these fringe packets are averaged with no weighting. The result is a single instrumental visibility for the source at the time of the observation. The standard deviation of the mean is taken to be the uncertainty in this measurement.

2.3. *Data Calibration*

We paired observations of δ^2 Lyrae with observations of α Lyrae. Although α Lyrae is resolved on a 22 m baseline at near-infrared wavelengths, we selected it as a calibration source for two reasons. Its angular diameter has been measured, and no other sources either unresolved or of known diameter and bright enough to be detected with our instrument were within 6° of δ^2 Lyrae. Observing close pairs of sources improves the duty cycle because less time is required to move the interferometer between sources and reduces the likelihood of introducing systematic errors into the data due to changes in the instrument response with the pointing of the siderostats.

We have adopted a limb-darkened diameter (LDD) of 3.22 ± 0.15 mas for α Lyrae. This LDD is the unweighted average of the LDDs determined from observations obtained at the Narrabri Intensity Interferometer (Hanbury Brown, Davis, & Allen 1974a) and the Mark III Optical Interferometer (Mozurkewich et al. 2001). The term "limb-darkened diameter" appears often in the literature and deserves some discussion here given the nature of this paper.

The monochromatic optical-depth radius, defined to be the distance of the $\tau_\lambda = 1$ layer from the center of the star, is a wavelength-dependent quantity (see Baschek et al. 1991 for details). In the case of a compact atmosphere, for which the geometric extension is negligible compared with the total dimension of the star, the optical-depth radii at all wavelengths are coincident. Interferometric observations, however, are sensitive to the limb-darkening (the shape of the CLV), which varies with wavelength, so the UDDs fit to interferometric data at different wavelengths must show some variation with wavelength (e.g., Mozurkewich et al. 1991). If the model used to "correct" the UDDs for limb-darkening accurately predicts the limb-darkening at all wavelengths, then the corrections result in the same diameter at all wavelengths. It is this diameter that is often referred to as the LDD in the literature. Hanbury Brown et al. (1974a) and Mozurkewich et al. (2001) have observed α Lyrae at different wavelengths and have used different models for α Lyrae, but the LDDs are in agreement to within their uncertainties, so we have chosen not to rework the original data

For computational ease, we have chosen to use a uniform-disk model to correct the observations of α Lyrae for partial resolution. The differences between the visibilities for a limb-darkened disk and its equivalent uniform disk are negligible at low spatial frequencies relative to the first null. Because our observations of α Lyrae occur at such low spatial frequencies, our choice of a uniform-disk model introduces negligible error into the calibration of the data. In order to use such a model, though, we require UDDs at 1.25 and 1.65 μm that are consistent with our adopted LDD.

We have adopted LDD to UDD ratios for α Lyrae of 1.020 and 1.015 at 1.25 and 1.65 μm, respectively. The procedure that we have used to arrive at these LDD to UDD ratios is an adaptation of the procedure that Hofmann & Scholz (1998) used to fit uniform disks to their model CLVs to arrive at their $R_{\rm UD}/R_{\rm fil}$ ratios. The salient features are as follows. The uniform disk and the model limb-darkened disk (or the model CLV) are compared with one another in the Fourier domain. Both the amplitude and radius of the uniform disk are adjusted until the least-squares difference between the visibilities of the two disks out to the first null reaches a minimum. The fit is subject to the constraint that the total integrated intensities of the two disks must be equal. The ratio of the two radii resulting from this procedure is the scaling factor that we use to convert between UDD and LDD.

Slight differences in scaling factors can result from different fitting techniques. A common alternate technique is to match the squares of the visibilities of the two disks at a single value. $V^2 = 0.3$ is typical because this is the point of the maximum rate of change in V^2 (e.g., Davis et al. 2000). Based on our experience, the differences in scaling factors that can arise from different fitting techniques are less than 1%–2% for the extended models discussed here and even less for the compact models (cf. Davis et al. 2000). In some extreme cases, though, the presence of water vapor or dust in the outermost layers of the atmosphere results in a two-component CLV (cf. Jacob et al. 2000; Bedding et al. 2001;

Scholz 2001). In these extreme cases, scaling factors are baseline dependent. From an observational perspective, if two interferometers with different baselines were to observe the same two-component CLV at the same wavelength, the UDDs resulting from the observations would be quite different. Certainly, this is not the case with α Lyrae, and we do not expect this to be the case with δ^2 Lyrae.

The limb-darkened disks representing α Lyrae at 1.25 and 1.65 μm were reconstructed from quadratic limb-darkening coefficients and the quadratic limb-darkening law given by Claret, Díaz-Cordovés, & Gimínez (1995) for a Kurucz model atmosphere with $\log g = 4.0$ and $T_{\rm eff} = 10{,}000$ K. The g and $T_{\rm eff}$ characterizing this model are within 2% of the g and $T_{\rm eff}$ given by Straizys & Kuriliene (1981) for an A0 V class star such as α Lyrae. In the near-infrared passbands, and at such high values of g and $T_{\rm eff}$, large differences in g and $T_{\rm eff}$ ($\pm 10\%$, for example) correspond to almost negligible differences ($\pm 0.1\%$) in the LDD-to-UDD ratios. The adopted LDD-to-UDD ratios yield UDDs for α Lyrae of 3.15 ± 0.14 and 3.17 ± 0.15 at 1.25 and 1.65 μm, respectively.

To calibrate the data then, each observation of α Lyrae is corrected for partial resolution using a uniform-disk model. The model parameters are the UDD for α Lyrae appropriate for the wavelength of the observation and the projected baseline of the interferometer at the time of the observation. The visibility obtained from this correction is divided into the instrumental visibility for δ^2 Lyrae to remove the effect of the constant components of the response functions of the instrument and the atmosphere. The result is the calibrated visibility for δ^2 Lyrae.

The uncertainty in the calibrated visibility for δ^2 Lyrae is taken to be the quadrature sum of four factors: (1) the uncertainty in the adopted UDD for α Lyrae, (2) the uncertainty in the instrumental visibility for α Lyrae, (3) the uncertainty in the instrumental visibility for δ^2 Lyrae, and (4) a measure of uncertainty that attempts to account for changes in the response functions of the instrument and the atmosphere that might have occurred during the course of the observations. The rms scatter in the instrumental visibilities for α Lyrae after correction for partial resolution during the period of time when no adjustments were made to the instrument is $\sim$3%. We have therefore adopted 3% as a representative value for this fourth factor in the uncertainty in the calibrated visibility for δ^2 Lyrae.

2.4. *UDDs for δ^2 Lyrae*

The instrumental visibilities for α Lyrae and δ^2 Lyrae are summarized in Table 1. The visibilities for α Lyrae corrected for partial resolution, the calibrated visibilities for δ^2 Lyrae, and the spatial frequencies for the observations are also summarized in Table 1. A uniform-disk model fit to the 1.25 μm data yields an angular diameter for δ^2 Lyrae of 10.33 ± 0.09 mas. A fit to the 1.65 μm data yields an angular diameter of 10.32 ± 0.10 mas. The uniform-disk diameter fits to the data are shown in Figures 1 and 2.

Additional interferometric observations of δ^2 Lyrae have appeared in the literature. Mozurkewich et al. (2001) observed δ^2 Lyrae at 0.550 μm ($\Delta\lambda = 0.025$ μm) and 0.800 μm ($\Delta\lambda = 0.025$ μm) using the Mark III Optical Interferometer. Quirrenbach et al. (1993) observed δ^2 Lyrae using the Mark III Optical Interferometer at 0.712 μm ($\Delta\lambda = 0.012$ μm) and 0.754 μm ($\Delta\lambda = 0.005$ μm), inside and outside a deep TiO absorption feature. These observations were part of a larger observational program to study the extended nature of the atmospheres of the coolest stars following the initial discovery of this phenomenon in Mira variables (Labeyrie et al. 1977). Dyck et al. (1998) observed δ^2 Lyrae using IOTA at 2.2 μm. The UDDs for δ^2 Lyrae reported here and in the literature are presented in Table 2. It is evident from Table 2 that the scatter in the UDDs for δ^2 Lyrae with wavelength significantly exceeds the published, formal uncertainties.

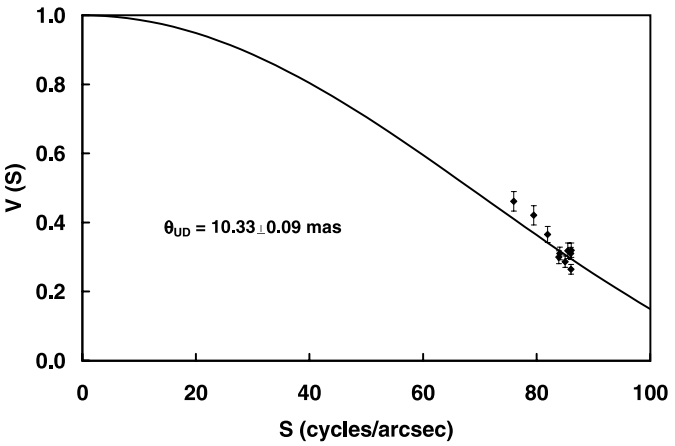

FIG. 1.—UDD fit to the calibrated visibility data for δ^2 Lyrae at 1.25 μm.

3. OBSERVATIONAL TESTS OF THE MODEL ATMOSPHERES

The variations in the UDDs with wavelength seen in Table 2 are expected. Our goal now is to test the most appropriate M class giant model atmosphere for δ^2 Lyrae against the data. Our test is quite simple. We scale the UDD in each passband to an RMD using the $R_{\rm UD}/R_{\rm Ross}$ ratio (the product of $R_{\rm UD}/R_{\rm fil}$ and $R_{\rm fil}/R_{\rm Ross}$) prescribed by the most appropriate model for the star. The RMD is a wavelength-independent quantity. If the RMDs across all wavelengths are in agreement with one another to within their uncertainties, then we have strong evidence toward the conclusion that the model provides a good description of the atmosphere of the star. First, though, the choice of an appropriate model deserves considerable attention.

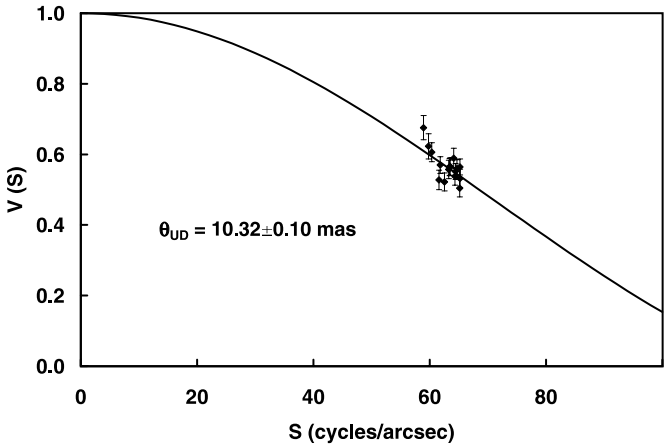

FIG. 2.—Same as Fig. 1, but at 1.65 μm

TABLE 2
COMPARISON OF MODEL FITS TO THE UDDS FOR δ^2 LYRAE

λ_{obs} (μm)	$\Delta\lambda_{obs}$ (μm)	Feature	θ_{UD}	γ_δ	$\theta_{Ross,\delta}$	γ_{X335}	$\theta_{Ross,X335}$
0.550	0.025	Weak TiO	9.932 ± 0.378	1.148	11.40 ± 0.43	1.180	11.72 ± 0.45
0.712	0.012	Weak to strong TiO	11.76 ± 0.30	1.110	13.05 ± 0.33	0.917	10.78 ± 0.28
0.754	0.005	Weak TiO	10.85 ± 0.26	1.077	11.69 ± 0.28	1.100	11.94 ± 0.29
0.800	0.025	Weak TiO	10.669 ± 0.107	1.067	11.38 ± 0.11	1.074	11.46 ± 0.11
1.25	0.30	Near-continuum	10.33 ± 0.09	1.050	10.84 ± 0.09	1.064	11.00 ± 0.10
1.65	0.30	Near-continuum	10.32 ± 0.10	1.053	10.87 ± 0.11	1.086	11.20 ± 0.11
2.20	0.40	Near-continuum	9.7 ± 0.3	1.034	10.03 ± 0.31	1.063	10.31 ± 0.32
θ_{mean}			10.55 ± 0.63		11.32 ± 0.94		11.20 ± 0.56
χ^2			35.6		90.9		27.7

NOTES.—The variable θ_{UD} represents the UDD for δ^2 Lyrae determined from interferometric observations (see text for references). Here γ_δ and γ_{X335} represent the R_{UD} and R_{Ross} ratios associated with the δ^2 Lyrae model (col. [3], Table 3) and the X335 model (col. [4], Table 3), respectively. The variables $\theta_{Ross,\delta}$ and $\theta_{Ross,X335}$ represent RMDs, where $\theta_{Ross,\delta} = \gamma_\delta\,\theta_{UD}$ and $\theta_{Ross,X335} = \gamma_{X335}\,\theta_{UD}$. The variable θ_{mean} represents the unweighted mean of the RMDs in each column, and χ^2 represents the scatter in the RMDs relative to θ_{mean}. Model passbands and observational passbands are not identical in all cases (see text for details).

Although δ^2 Lyrae is a variable star, the amplitude of variability is quite small ($\Delta m_V \approx 0.20$). The period is irregular, although strong modes have appeared at $\sim$60 and $\sim$100 days (Bakos & Tremko 1991). This star clearly does not belong to the class of Mira variables. Given the choice between a static model and a Mira model, the static model is expected to be the more appropriate choice.

Two parameters apart from the chemical composition are sufficient to characterize a static, plane-parallel model atmosphere: the surface gravity, g, and the effective temperature, T_{eff}. These parameters tie together three of the fundamental properties of a star: the mass, the radius, and the luminosity (Baschek et al. 1991). Three parameters, though, are required to characterize a static, spherically extended model atmosphere: g, T_{eff}, and a parameter that provides a measure of the extension of the atmosphere. In the M class giant models, the parameter $d = (r_0/R) - 1$, where R represents the distance from the center of the star at which $\tau_{Ross} = 1$ and r_0 represents the distance from the center at which τ_{Ross} reaches some negligible value (here 10^{-5}), describes the extension of the atmosphere. This extension parameter, however, is not an observable quantity and cannot be derived from observable quantities. Bessell et al. (1989a) have suggested using $D = T_{eff}/(gR)$, where T_{eff} is given in K, g in cm s^{-2}, and R in solar units, in real applications. The parameter D is a rough measure of model extension parameter d and can be derived from observations.

In order for us to compare δ^2 Lyrae to the available models, we must have estimates of g, T_{eff}, and D for δ^2 Lyrae. Rather than attempt to estimate these parameters from spectroscopic data, we have chosen to calculate these parameters from estimates of the mass, the radius, and the luminosity of δ^2 Lyrae, which we have calculated from observational data, except in the case of the mass, where we have consulted the results from the most recent calculations of the evolution of intermediate-mass stars.

The parallax of δ^2 Lyrae listed in the *Hipparcos* catalog is 3.63 ± 0.56 mas (Perryman et al. 1997). On the basis of this parallax measurement, the distance to δ^2 Lyrae is 275 ± 40 pc.

Given the distance to δ^2 Lyrae, we could calculate the linear diameter from the observed angular diameter of δ^2 Lyrae, but a single, definitive angular diameter is not available. Instead, we have a set of UDDs determined from interferometric observations. One of the core issues in this paper is the proper scaling between the UDDs determined from observations and a well-defined diameter associated with a model stellar atmosphere. Strictly speaking, we should calculate an RMD for the star based on the available data and a reasonable model for the star, then iterate through a series of adjustments to the model and the RMD until we reach a convergent solution for both. We show later, however, that other factors dominate the problem, and we ignore such an iterative procedure here. Instead, we adopt an angular diameter of 11.2 ± 0.6 mas for δ^2 Lyrae, in anticipation of our results. Given the distance to δ^2 Lyrae and this value for the angular diameter, we find the radius of δ^2 Lyrae to be $330 \pm 50\ R_\odot$.

Using Johnson broadband photometry (Morel & Magnenat 1978; Gezari et al. 1996) and assuming no reddening, we find the bolometric flux of δ^2 Lyrae to be $(5.96 \pm 0.18) \times 10^{-13}$ W cm^{-2}. Given the bolometric flux and the distance, we find the luminosity of δ^2 Lyrae to be $(1.4 \pm 0.3) \times 10^4\ L_\odot$. This luminosity is in agreement with the luminosity determined from the absolute visual magnitude (Wilson & Bappu 1957), $L = (1.2 \pm 0.5) \times 10^4\ L_\odot$.

Given the angular diameter and the bolometric flux, we find the effective temperature of δ^2 Lyrae to be 3460 ± 160 K. This value is consistent with the effective temperatures for the M class giants reported in the literature (Ridgway et al. 1980; Di Benedetto 1993; Dyck et al. 1996, 1998; Richichi et al. 1999; van Belle et al. 1999).

To arrive at an estimate for the mass of δ^2 Lyrae, we have consulted the results of the most recent calculations of the evolution of intermediate-mass stars. Thomas Blöcker (1999, private communication) has plotted for us the luminosities and effective temperatures for a grid of model stars between 3 and 6 $M_\odot$ from the start of the main-sequence stage of evolution through to the final stages of evolution on the asymptotic giant branch (AGB). All of the stars in the grid have solar composition, and the evolution of the stars includes mass loss (e.g., Blöcker 1995). Comparing the luminosity and effective temperature of δ^2 Lyrae with the luminosities and effective temperatures of the model stars, we estimate the initial mass of δ^2 Lyrae to be $5.5 \pm 1.0\ M_\odot$. This value is consistent with the value that one obtains from an interpolation of the model data in the tables in Bessell et al. (1989a, 1991). Mass-loss estimates for δ^2 Lyrae range

between 10^{-7} and 10^{-8} $M_\odot$ yr^{-1} (Sanner 1976a; Hagen, Stencel, & Dickinson 1983; de Jager, Nieuwenhuijzen, & van der Hucht 1988), and the environment around δ^2 Lyrae appears to contain little dust (Hagen, Stencel, & Dickinson 1983; Heske 1989). The total mass loss up until now, according to the model evolution, has been negligible relative to the total mass of the star, which is consistent with observations, so we can take the initial mass to be the present mass without significant error.

Given the mass, the radius, and the effective temperature for δ^2 Lyrae, we find $\log g = 0.14^{+0.07}_{-0.09}$ and $D = 7.61 \pm 1.87$. Straizys & Kuriliene (1981) find $\log g = 0.20$ for a star of spectral type M4 II, somewhat higher than our result, but still in agreement within the uncertainty. We must note, though, that the Straizys & Kuriliene result for g depends on a semiempirical relationship among M, g, $T_{\rm eff}$, and $M_{\rm bol}$. We refer the reader to Vardya (1976) for a discussion of this relationship and the potential pitfalls of the application of this relationship to stars with extended atmospheres.

In the absence of adequate calibrated spectroscopic data, we assume solar abundances for δ^2 Lyrae (B. J. Taylor 1999, private communication; see also Taylor 1999 and Cayrel de Strobel et al. 1997). All of the parameters for δ^2 Lyrae presented above are summarized in Table 3.

Hofmann & Scholz (1998) have published $R_{\rm UD}/R_{\rm fil}$ and $R_{\rm fil}/R_{\rm Ross}$ ratios in eight narrow and four broad photometric bands for a subset of the static, spherically extended, M class giant model atmospheres that appear in Bessell et al. (1989a, 1991). Although numerous models between 1 and 15 $M_\odot$ are available, Hofmann & Scholz limited their study to the 1 $M_\odot$ models of solar composition, referred to as the X, Z, and U series of models. These models have luminosities of 1×10^4 $L_\odot$, 2×10^3 $L_\odot$, and 5×10^2 $L_\odot$, respectively. The effective temperatures of the models range from 3500 to 2500 K.

None of these models, though, match δ^2 Lyrae in g, $T_{\rm eff}$, and D. The X, Z, and U series model atmospheres are more extended than δ^2 Lyrae, at least on the basis of our calculations above, so interpolation of the models is not warranted. None of the other static models in Bessell et al. (1989a, 1991) are a good match to δ^2 Lyrae either, so we computed a new model matching δ^2 Lyrae in mass, radius, and luminosity for this project. The parameters of this particular model, hereafter the δ^2 Lyrae model, are summarized in Table 3. To arrive at $R_{\rm UD}/R_{\rm Ross}$ ratios for the δ^2 Lyrae model, we fitted uniform disks to the model CLVs using the same routine presented in § 2 in the discussion of the calibration of the interferometric data.

TABLE 3
Comparison of Stellar and Model Characteristics

Parameter (1)	δ^2 Lyrae (2)	δ^2 Lyrae Model (3)	X335 Model (4)
M ($M_\odot$).....	5.5 ± 1.0	5.5	1.0
R ($R_\odot$).....	332 ± 52	332	298
L ($L_\odot$).....	$1.37 \pm 0.30 \times 10^4$	1.37×10^4	1.0×10^4
Z ($Z_\odot$).....	1.0	1.0	1.0
$T_{\rm eff}$ (K).....	3460 ± 160	3430	3350
$\log g$ (cgs).....	0.14 + 0.07−0.09	0.136	−0.51
D.....	7.61 ± 1.87	7.55	36.4
d.....		0.06	0.51

Notes.—The second column lists the characteristics of δ^2 Lyrae as determined from a combination of empirical and theoretical data (see § 3 of the text for details). The third and fourth columns list the parameters for the two model stellar atmospheres discussed in the text. The parameter D is given in K cm^{-1} s^2 $R_\odot^{-1}$, and the parameter d represents the opacity-dependent extension of the model atmospheres (see § 3 of the text for details).

Model computations were performed in the same 12 passbands defined in Hofmann & Scholz (1998). Not all of the observational passbands, though, are represented in the model. To arrive at the $R_{\rm UD}/R_{\rm Ross}$ ratios at 0.550, 0.800, and 1.25 μm, we interpolated the $R_{\rm UD}/R_{\rm Ross}$ ratios in neighboring continuum or near-continuum passbands. Based on the variations in the $R_{\rm UD}/R_{\rm Ross}$ ratio with wavelength in continuum or near-continuum portions of the spectrum (cf. Jacob et al. 2000), we do not expect these interpolations to have introduced errors larger than ~1%. We have also applied the $R_{\rm UD}/R_{\rm Ross}$ ratio at 0.710 μm to the UDD at 0.712 μm. The 0.710 μm filter in the model computations has a width of 0.001 μm, whereas the observational passband at 0.712 μm has a width of 0.012 μm. These passbands lie in a region of the spectrum dominated by TiO absorption features, so the mismatch between the model and the observational passbands is a concern. To address this concern, we have also computed the $R_{\rm UD}/R_{\rm Ross}$ ratio for the δ^2 Lyrae model and a second model, the X335 model, which we introduce later in the paper, in a 0.012 μm wide passband at 0.712 μm. The $R_{\rm UD}/R_{\rm Ross}$ ratio in this passband is ~2% larger than at 0.710 μm for both models. We use the $R_{\rm UD}/R_{\rm Ross}$ ratio at 0.710 μm here for the sake of consistency with all of the other models tested against the data and note that a more accurate representation of the $R_{\rm UD}/R_{\rm Ross}$ ratio at 0.712 μm has little effect on our results.

The UDDs for δ^2 Lyrae, the $R_{\rm UD}/R_{\rm Ross}$ ratios in the observational passbands, and the resulting RMDs appear in Table 2. The unweighted mean RMD is 11.3 ± 1.0 mas. The χ^2 of the RMDs about the unweighted mean is 90.9.

We have chosen to work with unweighted mean diameters as opposed to weighted mean diameters because the UDDs were determined from data obtained at three different interferometers. A systematic error or a poor estimate of the uncertainty in one or more of the UDDs could skew the agreement between a particular model and the data. The χ^2 about the mean provides a useful measure of the scatter in the data and the quality of the agreement between the model and the data. For comparison, the χ^2 of the UDDs about the unweighted mean UDD is 35.6.

If the δ^2 Lyrae model were an accurate description of the atmosphere of δ^2 Lyrae, we would expect the RMDs to be in agreement with one another to within their uncertainties. We would also expect the χ^2 of the RMDs about the mean to be on the order of the number of independent diameter measurements, or ~7.0. We must conclude that either the δ^2 Lyrae model does not adequately describe the atmosphere of this particular star or the data are suspect, a subject to which we will return in § 4.

This result prompted us to test all of the X, Z, and U series models against the data. From the point of view of a χ^2 minimization, the X335 model provides the "best fit" to the data. The parameters of this model are listed in Table 3. The UDD data for δ^2 Lyrae, the $R_{\rm UD}/R_{\rm Ross}$ ratios in the observational passbands, and the resulting RMDs for δ^2 Lyrae appear in Table 2.

The unweighted mean RMD is 11.2 ± 0.6 mas. The χ^2 of the RMDs about the unweighted mean RMD is 27.7, more than a factor of 3 better than the δ^2 Lyrae model, and almost

a factor of 2 better than the next best model in the X, Z, and U series of models. The agreement amongst the RMDs, although much improved, is still not satisfactory, and we cannot conclude that the X335 model provides an adequate description of the atmosphere of δ^2 Lyrae. The fact that the X335 model provides a much better fit to the data than the δ^2 Lyrae model is nonetheless instructive and serves as the foundation for the discussion in the next section. Based on our experience with these models, we have adopted 11.2 ± 0.6 mas as the best current estimate available for the RMD of δ^2 Lyrae.

4. DISCUSSION

On the one hand, we have a model that is a close match to δ^2 Lyrae with regard to the fundamental stellar properties of mass, radius, and luminosity, but this model cannot account for the interferometric data. On the other hand, we have a model that can account for the data much better than all of the other models available, but this model has a much lower mass and a much more extended atmosphere than expected for δ^2 Lyrae. There are several possible explanations for these results.

Let us assume for the moment that the static picture is correct. The relative success of the X335 model then brings into question our mass estimate for δ^2 Lyrae. Is δ^2 Lyrae in fact a low-mass star? Our mass estimate is based on a comparison of the L and $T_{\rm eff}$ for δ^2 Lyrae to the luminosities and effective temperatures for a grid of model stars between 3 $M_\odot$ and 6 $M_\odot$ throughout their evolution from the main-sequence stage of evolution through to the final stages of evolution on the AGB. In the region where we find δ^2 Lyrae, the evolutionary tracks for the grid stars parallel one another, and the tracks for stars 1 $M_\odot$ apart differ by $\sim$50% in L (at a fixed $T_{\rm eff}$) and $\sim$5% in $T_{\rm eff}$ (at a fixed L). These differences are on the order of the uncertainties in the L and $T_{\rm eff}$ for δ^2 Lyrae. The tracks for stars less than 3 $M_\odot$ must lie at lower luminosities and effective temperatures. If δ^2 Lyrae is in fact a 1 $M_\odot$ star, then our estimate of either the luminosity or the effective temperature must be in error by more than three standard deviations. Although not impossible, it is quite improbable that this is the case.

Perhaps, though, the critical difference between the δ^2 Lyrae model and the X335 model is not the difference in mass but the different degrees to which the atmospheres are extended. Let us assume for the moment that the δ^2 Lyrae model is the most appropriate model because it matches δ^2 Lyrae in mass, radius, and luminosity. The relative success of the X335 model then suggests that the δ^2 Lyrae model might account for the data if the model were to have a much more extended atmosphere. In a static model, however, the extension of the atmosphere cannot be changed without changing the mass, the radius, or the luminosity (or some combination of these three parameters), or adding an artificial mechanism to alter the temperature-density stratification of the atmosphere.

The star δ^2 Lyrae is a small amplitude, red variable. Variability suggests pulsation, and pulsation can cause some "levitation" of the atmosphere (Willson 2000), which it is most remarkable in the case of the Mira variables. The observational evidence for pulsation in δ^2 Lyrae is not conclusive. Although mass loss is evident (Sanner 1976b; Hagen et al. 1983), mass loss does not require pulsation, and the *IUE* data for δ^2 Lyrae do not show the signature of pulsation (Eaton, Johnson, & Cadmus 1990).

There are other points to consider, however. Our data set is not homogeneous. The UDDs reported here were determined from interferometric data obtained at three different interferometers between 1988 and 1998. Changes in both the period and the structure of the light curve of δ^2 Lyrae occurred during an 8 year period of observations in the 1980s (Bakos & Tremko 1991). Sufficient data are not available to determine whether or not this irregular behavior has persisted. The observations from the 1980s suggest, though, that changes in the structure of the atmosphere of δ^2 Lyrae might occur on timescales less than $\sim$1 yr. We therefore cannot rule out the possibility that the UDDs for δ^2 Lyrae presented here reflect not just differences in limb-darkening at different wavelengths, but also changes in the structure of the atmosphere with time.

Given the different origins of the UDD estimates at optical and near-infrared wavelengths, and given the small number of UDD estimates, a systematic error or a poor estimate of the uncertainty in one or more UDDs could have a strong influence on the apparent quality of the fits of the models to the UDDs. Nordgren, Sudol, & Mozurkewich (2001) have shown that there are no systematic differences between the diameters obtained at the Mark III Optical Interferometer and the NPOI at optical wavelengths. Nordgren et al. have also shown that the quoted uncertainties in the diameters are in good agreement with statistical differences between the diameters from the two interferometers. It is therefore reasonable to accept as accurate the UDDs for δ^2 Lyrae at optical wavelengths, all of which were determined from the observations made at the Mark III Optical Interferometer.

The near-infrared beam combiner at the NPOI, however, represents a different optical system with different performance characteristics than the optical beam-combiner at the NPOI, so the same arguments that apply to the UDDs at optical wavelengths do not apply to the UDDs at 1.25 and 1.65 μm. Furthermore, UDDs determined from interferometric data obtained on a single baseline are more susceptible to errors than those determined from multiple baseline data (e.g., Nordgren et al. 1999; Mozurkewich et al. 2001). Errors can arise as a result of poor calibration of the visibilities or as a result of having observed a source with an unusual CLV in a narrow range of spatial frequencies (cf. Jacob et al. 2000; Bedding et al. 2001; Scholz 2001; Jacob & Scholz 2002). We have no reason to suspect that the CLVs for δ^2 Lyrae in the observational passbands presented here are so unusual that the UDDs are baseline dependent in addition to being wavelength dependent. On the other hand, sufficient data are not available to assess whether or not systematic calibration errors are present in the UDDs at 1.25 and 1.65 μm. The same arguments, more or less, apply to the UDD at 2.2 μm from IOTA.

If we treat the near-infrared UDDs as suspect and compare the models to the UDDs at optical wavelengths alone, we find that the models still cannot account for the variations in the UDDs with wavelength; $\chi^2 = 33.2$ for the δ^2 Lyrae model, and $\chi^2 = 9.2$ for the X335 model. It is clear, though, that the near-infrared UDDs do make a large contribution to χ^2. Rather than ignore the near-infrared UDDs altogether, we might instead increase the uncertainties in the near-infrared UDDs to accommodate potential errors. If we triple the uncertainties in the near-infrared UDDs (to $\sim$3% at 1.25 and 1.65 μm and $\sim$9% at 2.20 μm), we find

again that the models cannot account for the variations in the UDDs with wavelength; $\chi^2 = 35.9$ for the δ^2 Lyrae model, and $\chi^2 = 16.7$ for the X335 model. The point of these simple exercises is that the disagreement between each of the models and the UDDs is large and in all likelihood not entirely the result of systematic calibration errors.

One last point to consider is that observations in line-blanketed passbands are most sensitive to the temperature-density stratification of the atmosphere. However, the model CLVs are most sensitive to the details of the modeling in these same passbands. The model predictions depend on the completeness and accuracy of the molecular line data and the technique used to treat the line contributions to the CLV in the passband. This has the most significant impact on the observation of δ^2 Lyrae in the TiO band at 0.712 μm, but the resolution of the disagreement between the predictions of the models and the UDDs cannot lie in this point alone. Tied to this problem is the problem of the true composition of δ^2 Lyrae. We have had to assume that δ^2 Lyrae is a star of solar composition. To determine whether or not composition is important in the case of δ^2 Lyrae, observational estimates of the metallicity of δ^2 Lyrae are needed, and perhaps more extensive modeling of this star, but that is beyond the scope of this paper.

The most reasonable conclusion that we can render from the disagreement between the model predictions and the UDDs for δ^2 Lyrae is that the atmosphere of δ^2 Lyrae and perhaps the atmospheres of all similar small amplitude, red variable stars cannot be adequately described with a static model atmosphere. There are a number of possible alternate explanations, though, for this disagreement and combinations of these alternatives, which cannot be ignored.

5. CONCLUSION

This work illustrates an important disagreement between the UDDs for δ^2 Lyrae determined from interferometric observations at optical and near-infrared wavelengths and the predictions of static, spherically extended model atmospheres for the M class giants. The disagreement between the UDDs for δ^2 Lyrae and the models suggests that even in a small-amplitude, red variable star, dynamic mechanisms in the atmosphere have a significant effect on the temperature-density stratification such that a static model cannot provide an adequate description of the atmosphere. This work further illustrates the difficulty in the interpretation of interferometric observations of M class giants but shows the power of interferometric data as a diagnostic tool in the evaluation of theoretical models of stellar atmospheres.

In comparison to results for hotter stars, we are unable to derive a satisfactory wavelength-independent measure of the angular diameter of δ^2 Lyrae. In our best judgement, the RMD for δ^2 Lyrae is 11.2 ± 0.6 mas. Until more data are available for a larger sample of stars, and until the discrepancies between the data and the models can be resolved, the accuracy with which we can determine the angular diameters of the coolest stars will likely be limited to $\sim$5%.

We thank Thomas Blöcker, who provided us with evolutionary tracks for intermediate-mass stars and some critical comments regarding our mass estimate for δ^2 Lyrae. We thank Lee Anne Wilson, who provided some critical comments on atmospheric extension in stars exhibiting mass loss. We also thank Cathy Sachs, Ben Burress, and Bob Thompson for their assistance during observing runs at the NPOI.

REFERENCES

Armstrong, J. T., et al. 1998, ApJ, 496, 550
Bakos, G. A., & Tremko, J. 1991, Cont. Astron. Obs. Skalnate Pleso, 21, 99
Baschek, B., Scholz, M., & Wehrse, R. 1991, A&A, 246, 374
Bedding, T. R., Jacob, A. P., Scholz, M., & Wood, P. R. 2001, MNRAS, 325, 1487
Benson, J. A., Dyck, H. M., & Howell, R. R. 1995, Appl. Opt., 34, 51
Bessell, M. S., Brett, J. M., Scholz, M., & Wood, P. R. 1989a, A&AS, 77, 1 (erratum 87, 621)
———. 1989b, A&A, 213, 209
———. 1991, A&AS, 89, 335
Bessell, M. S., Scholz, M., & Wood, P. R. 1996, A&A, 307, 481
Blöcker, T. 1995, A&A, 297, 727
Cayrel de Strobel, G., Soubiran, C., Friel, E. D., Ralite, N., & François, P. 1997, A&AS, 124, 299
Claret, A., Díaz-Cordovés, J., & Giménez, A. 1995, A&AS, 114, 247
Davis, J., Tango, W. J., & Booth, A. J. 2000, MNRAS, 318, 387
de Jager, C., Nieuwenhuijzen, H., & van der Hucht, K. A. 1988, A&AS, 72, 259
Di Benedetto, G. P. 1993, A&A, 270, 315
Dyck, H. M., et al. 1995, AJ, 109, 378
Dyck, H. M., Benson, J. A., & Ridgway, S. T. 1993, PASP, 105, 610
Dyck, H. M., Benson, J. A., van Belle, G. T., & Ridgway, S. T. 1996, AJ, 111, 1705
Dyck, H. M., van Belle, G. T., & Thompson, R. R. 1998, AJ, 116, 981
Eaton, J. A., Johnson, H. R., & Cadmus, R. R. 1990, ApJ, 364, 259
Gezari, D. Y., Pitts, P. S., Schmitz, M., & Mead, J. M. 1996, The Catalog of Infrared Observations (version 3.5; Greenbelt, MD: GSFC)
Hagen, W., Stencel, R. E., & Dickinson, D. F. 1983, ApJ, 274, 286
Hajian, A. R., et al. 1998, ApJ, 496, 484
Hanbury Brown, R., Davis, J., & Allen, L. R. 1974a, MNRAS, 167, 121
Hanbury Brown, R., Davis, J., Lake, R. J. W., & Thompson, R. J. 1974b, MNRAS, 167, 475
Haniff, C. A., Scholz, M., & Tuthill, P. G. 1995, MNRAS, 276, 640
Heske, A. 1989, A&A, 208, 77
Hofmann, K.-H., Balega, Y., Scholz, M., & Weigelt, G. 2000, A&A, 353, 1016
———. 2001, A&A, 376, 518
Hofmann, K.-H., & Scholz, M. 1998, A&A, 335, 637
Hofmann, K.-H., Scholz, M., & Wood, P. R. 1998, A&A, 339, 846
Jacob, A. P., Bedding, T. R., Robertson, J. G., & Scholz, M. 2000, MNRAS, 312, 733
Jacob, A. P., & Scholz, M. 2002, MNRAS, submitted
Kurucz, R. L. 1979, ApJS, 40, 1
Labeyrie, A., Koechlin, L., Bonneau, D., Blazit, A., & Foy, R. 1977, ApJ, 218, L75
Morel, M., & Magnenat, P. 1978, A&AS, 34, 477
Morgan, W. W., & Keenan, P. C. 1973, ARA&A, 11, 29
Mozurkewich, D., et al. 1991, AJ, 101, 2207
———. 2001, AJ, submitted
Nordgren, T. E., et al. 1999, AJ, 118, 3032
Nordgren, T. E., Sudol, J. J., & Mozurkewich, D. 2001, AJ, 122, 2707
Perrin, G., et al. 1999, A&A, 345, 221
Perryman, M. A. C., et al. 1997, A&A, 323, L49
Quirrenbach, A., Mozurkewich, D., Armstrong, J. T., Buscher, D. F., & Hummel, C. A. 1993, ApJ, 406, 215
Quirrenbach, A., Mozurkewich, D., Buscher, D. F., Hummel, C. A., & Armstrong, J. T. 1996, A&A, 312, 160
Richichi, A., Fabbroni, L., Ragland, S., & Scholz, M. 1999, A&A, 344, 511
Ridgway, S. T., Joyce, R. R., White, N. M., & Wing, R. F. 1980, ApJ, 235, 126
Sanner, F. 1976a, ApJ, 204, L41
———. 1976b, ApJS, 32, 115
Scholz, M. 1985, A&A, 145, 251
———. 2001, MNRAS, 321, 347
Scholz, M., & Takeda, Y. 1987, A&A, 186, 200 (erratum 196, 342)
Straizys, V., & Kuriliene, G. 1981, Ap&SS, 80, 353
Taylor, B. J. 1999, A&AS, 135, 75
van Belle, G. T., et al. 1999, AJ, 117, 521
Vardya, M. S. 1976, Ap&SS, 41, L1
Weigelt, G., Balega, Y., Hofmann, K.-H., & Scholz, M. 1996, A&A, 316, L21
Willson, L. A. 2000, ARA&A, 38, 573
Wilson, O. C., & Bappu, M. K. V. 1957, ApJ, 125, 661